The derivation of an analytical wake model from a parameterised study of the CFD-computed flow-fields behind a wind turbine

Bryan Nelson*, Tsung-yueh Lin
CR Classification Society University
bnelson@crclass.org

Abstract

Utility-scale wind energy is typically harnessed by wind farms, comprising dozens if not hundreds of wind turbines working together to generate electricity. Grouping wind turbines together in this way allows for a reduced levelised cost of electricity (LCOE), but also introduces new design problems, such as inter-turbine flow interactions, or "wake effects", which are known to reduce the wind farms' total output power, while simultaneously increasing the fatigue loading of the downstream wind turbines. There are many analytical wake models in current use which have, over the years, been shown to adequately predict the flow-fields through large wind farms under very specific conditions. However, many of these wake models are based on one-dimensional momentum theory, which neglects frictional drag and assumes a non-rotating wake, and, as such, these models are not appropriate for non-optimum operating conditions. To address these shortcomings, we are developing an analytical wake model, derived from unsteady, 3D, full-rotor CFD simulations of the flow field behind a single wind turbine for its full range of operating conditions. This paper describes our CFD model setup, the parameterisation of our CFD model results, and the validation of the CFD-based analytical model against site data from the literature, as well as against data predicted using commercial tools.

Keywords: wind farm, wake effects, CFD, flow field, energy yield assessment

I. Introduction

In order to increase energy security and decrease carbon emissions, Taiwan's Ministry of Economic Affairs' (MOEA) has been aggressively promoting the development of a localised renewable energy industry. Due to the island nation's world-class wind resources, the MOEA has focused their attention on the development of the local wind energy industry, recently raising their 2025 installed offshore capacity target to 5.7 GW, with an estimated total investment of around NT$ 1 trillion [1].

The planning, development, and financing of large-scale wind energy projects, such as the MOEA's "Thousand Wind Turbines" project, necessitate accurate, reliable tools for energy yield and wind-load assessments so as to reduce risk and maximise return on investment. These assessments are complicated by so-called wake effects, such as wake shadowing and wake meandering [2], which severely reduce the amount of wind energy available to the turbines located in the wakes of the upstream turbines, thereby diminishing the total power production of the wind farm. Moreover, the increased turbulence in the wakes results in increased load fluctuations (fatigue loading) [3]. To address these issues, we are currently developing a new analytical wake model which focuses on the relationship between the velocity deficit in the wake and the wind turbine thrust coefficient.

II. Jensen's wake model

One of the earliest wake models still in common use is that proposed by N.O. Jensen in 1983 [4]. It is a very simple model, assuming a linearly expanding wake, with a velocity deficit that is a function of the distance behind the rotor x and the wind turbine thrust coefficient C_T. The diameter of the wake D_w at a downstream distance x is given by:

$$D_w = D(1 + 2ks) \tag{1}$$

and the velocity in the (fully developed) wake is given by

$$u = U_\infty \left[1 - \frac{1 - \sqrt{1 - C_T}}{(1 + 2ks)^2}\right] \tag{2}$$

where D is the rotor diameter, U_∞ is the far-field velocity, $s = x/D$ is the non-dimensionalised distance behind the rotor, and the Wake Decay Constant is set as $k = 0.04$, which corresponds to the case of low atmospheric turbulence (TI = 8%) [5]. Despite its simplicity, the Jensen wake model has been shown to be very reliable [6], and is the default model adopted by Risø DTU's WAsP, GH's WindFarmer, UL's OpenWind, and EMD's WindPRO, to name a few.

For the case of multiple wakes, the present study employs the "sum of squares of velocity deficits" wake combination model proposed by Katic [7]:

$$\left(1 - \frac{u_j}{U_\infty}\right)^2 = \sum_i^N \left(1 - \frac{u_{ji}}{u_i}\right)^2 \frac{A_{\mathrm{shadow},i}}{A_0} \tag{3}$$

where u_j is the wind speed at turbine j due to all upstream turbines, u_i is the wind speed at upstream turbine i, u_{ji} is the wind speed at turbine j due to the wake of turbine i, and the summation is taken over the N turbines upstream of turbine j. For the case of partially overlapped wakes, the velocity deficit is weighted by the fraction of the overlapping area A_{shadow} to the rotor area of the down-stream turbine A_0. For the standard Jensen wake model, which assumes a uniform velocity profile, A_{shadow} may be calculated analytically [8]. However, to allow us to incorporate different velocity distributions into our wake model, we decided to calculate A_{shadow} numerically, by discretising the rotor/wake-overlap plane into a Cartesian grid (Figure 1).

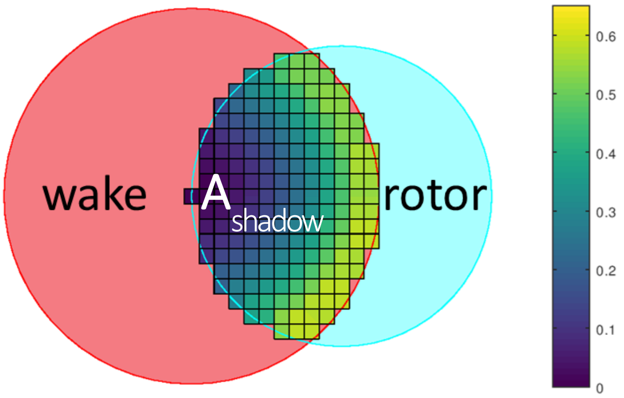

Figure 1. The wake-overlap area A_{shadow} is calculated by discretising the rotor/wake plane (cosine velocity distribution)

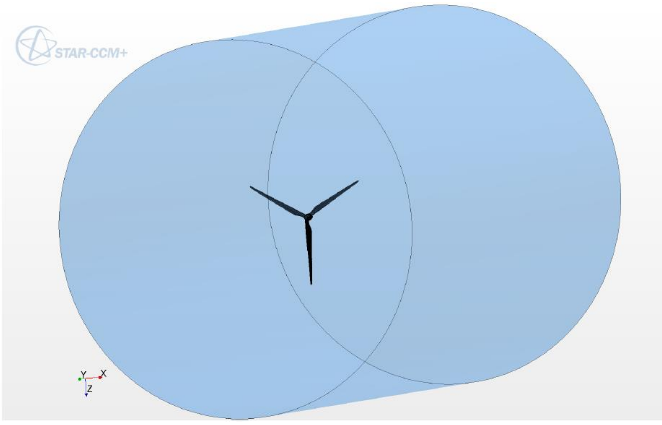

Figure 2. Computational domain for unsteady 3D full CFD simulation

II. Proposed wake model

Despite its impressive track record, Jensen's model suffers from two significant shortcomings, both of which stem from its basis in one-dimensional momentum theory. The first of these limitations is that 1-D momentum theory, and consequently Jensen's wake model, is not valid for $C_T > 1$, as may be seen from Equation (2). This condition, though not overly common, may be observed at low wind speeds for a non-negligible number of commercial wind turbines [11]. The second limitation stems from two of 1-D momentum theory's key assumptions, namely (1) no frictional drag, and (2) a non-rotating wake. While these assumptions may be appropriate at optimum operating conditions (i.e. around rated wind speed), the effects of frictional drag and the rotating wake may not be neglected at high tip-speed-ratios (low-to-negative angles of attack) and at low tip-speed-ratios, where the blades are pitched to maintain constant power and to reduce aerodynamic loading.

In order to overcome the above-mentioned limitations, we are currently developing a new analytical wake model which focuses on the numerically calculated relationship between the velocity deficit in the wake and the wind turbine's thrust coefficient. To this end, we have performed a number of unsteady 3D full-rotor CFD simulations, using the commercial RANS-based code STAR-CCM+. The modelled domain is illustrated in Figure 2, and a view of the surface mesh on the wind turbine hub and blades is shown in Figure 3. The computational domain has a diameter of four rotor diameters (4D), and extends two rotor diameters (2D) upstream, and eight rotor diameters (8D) downstream.

The target wind turbine for this study was the NREL 5 MW reference turbine, and our CFD results were validated against the power and thrust coefficients provided in the target wind turbine's documentation [12]. Figure 4 shows that there is excellent agreement between the two sets of power data and thrust coefficients, giving us confidence that our mesh resolution near the wind turbine is sufficiently fine.

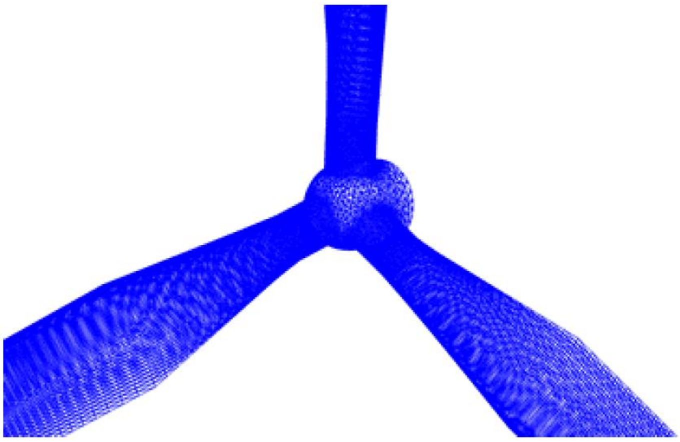

Figure 3. Surface mesh on the wind turbine hub and blades

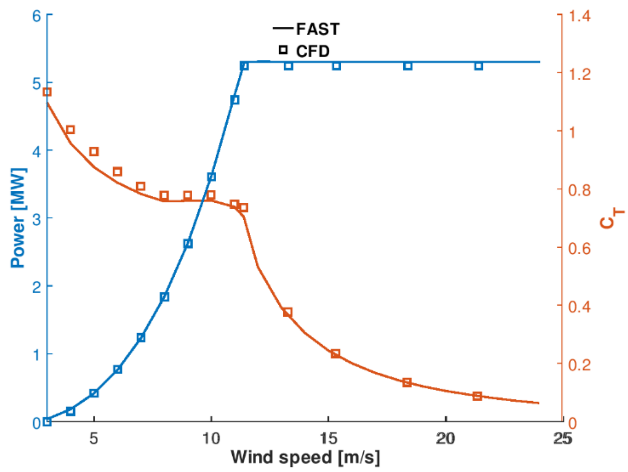

Figure 4. Validation of CFD results for Power and Thrust curves

However, to increase our confidence in the validity of the results throughout the downstream wake region, we performed a mesh independence assessment, running a number of different mesh configurations, some of which are shown in Figure 5, together with their respective mesh counts, and then parametrically analysing the wake profiles (circumferentially-averaged velocity distributions) at several downstream locations (Figure 6).

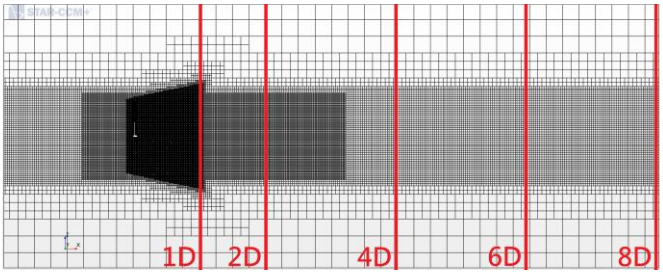

Mesh A (7 million cells)

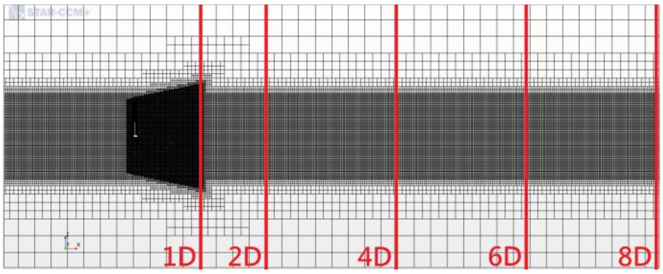

Mesh B (9 million cells)

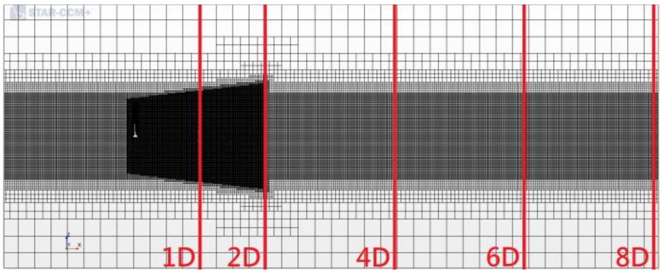

Mesh C (12 million cells)

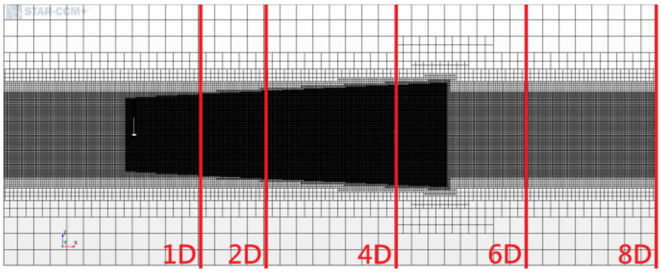

Mesh D (20 million cells)

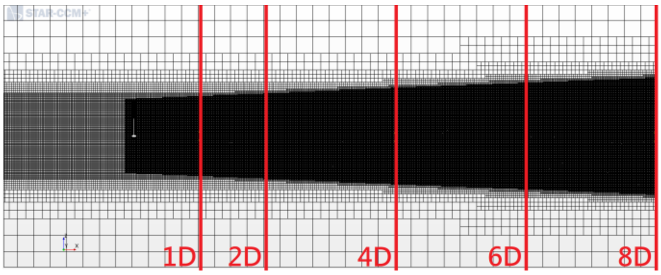

Mesh E (32 million cells)

Figure 5. Mesh configurations for mesh independence assessment (Not pictured: Mesh F, which resembles Mesh E, has 50M cells)

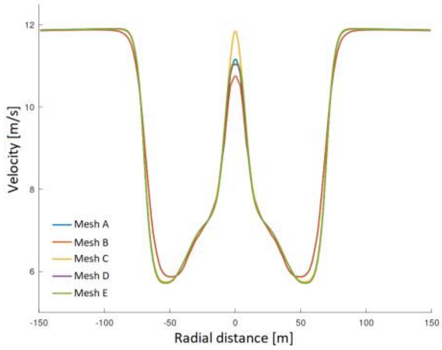

(a) 2D

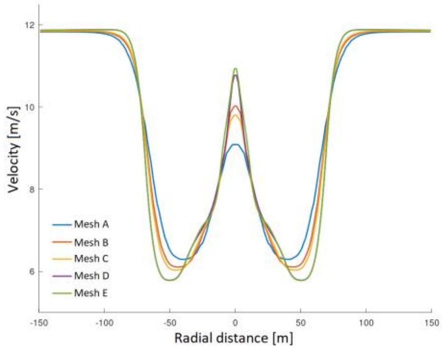

(b) 4D

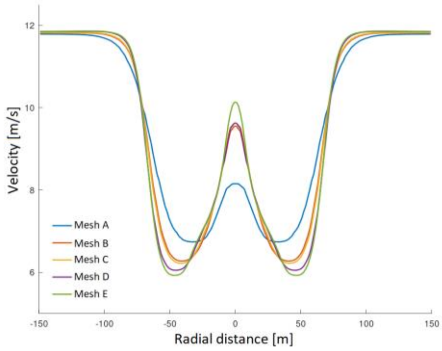

(c) 6D

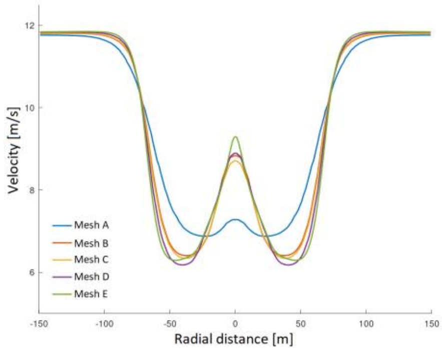

(d) 8D

Figure 6. Wake profiles (circumferentially-averaged velocity distribution) for mesh independence assessment

The results of the mesh independence assessment clearly show that finer mesh resolutions produced more pronounced wake profiles, with greater velocity deficits, higher wake-core velocities, as well as sharper transitions from free-stream velocity to wake velocities. The contrast is especially evident in our coarsest mesh, Mesh A, which significantly underpredicted the velocity deficit in the far-wake, while overpredicting the wake expansion, i.e. the diameter of the wake profile. On the other hand, it appears that extending the very fine volumetric control region to around 4D downstream (Mesh D) produces very similar results to those attained by extending the volumetric control throughout the computational domain.

To more quantitatively assess the mesh independence, we compared the deficit of volumetric flow rate in the wake ΔQ, (Equation 6) which was computed by radially integrating the wake velocity deficit $\Delta u = U_\infty - u_w$. These results, shown in Figure 7, are clearly seen to converge in meshes D, E, and F. It was therefore decided to adopt Mesh D for the full range of operating conditions.

$$\Delta Q = \int_0^{r_w} \Delta u \, dr \tag{4}$$

The next step was to parameterise the wake profile and find a curve to fit the wake's geometric features while also matching its flow rate deficit, ΔQ. This was achieved by segmenting the wake velocity profile at its extrema (namely the wake-core spike, the maximum velocity deficit, and the maximum velocity outside the wake region, demarcated by the three black squares 1 ~ 3 in Figure 8). The abscissae/ordinates of each segment were then min-max normalised, and nonlinear functions of the form

$$f(\hat{r}) = \hat{u}_N - \mathrm{sign}(\hat{u}_N - \hat{u}_1)(1 - \hat{r}^a)^b \tag{5}$$

were fit to the data by nonlinear least-squares regression analysis, where $\hat{r}$ is the normalised radial distance along the segment, $\hat{u}_N$ and $\hat{u}_1$ are, respectively, the normalised velocities at the outermost and innermost endpoints of the segments, and exponents a and b are determined by the regression analysis. A sample fit curve is included as a dotted line in Figure 8.

All maximum velocity deficit $\Delta u|_{\max}$ (Node 2) data and maximum velocity $u_{\max}$ (Node 3) data, normalised against the ambient wind speed U_∞, were then plotted against U_∞ (Figures 9 and 10), revealing a very strong relationship with the target turbine's thrust coefficient curve (recall Figure 4), as well as a nonlinear effect dependent on the downwind distance s.

Plotting the radial coordinates of Nodes 2 and 3 against U_∞ (Figures 12 and 13) once again reveals a strong relationship with C_T, although the effects of downstream distance s are far more pronounced here. This is to be expected, however, since the problem of wake expansion downwind of an operational wind turbine is one of the key issues under investigation in this study.

To further investigate the effects of the downwind distance s on the wake velocity and wake diameter, the normalised velocity and location data at Node 3 were plotted against s (Figures 11 and 14). These two figures clearly illustrate the nonlinearity of the effects of the s parameter, in terms of both wake velocity recovery (Figure 11) and wake expansion (Figure 14), while highlighting a further complication: two distinct regions of influence, namely pre-rated wind speed and post-rated wind speed.

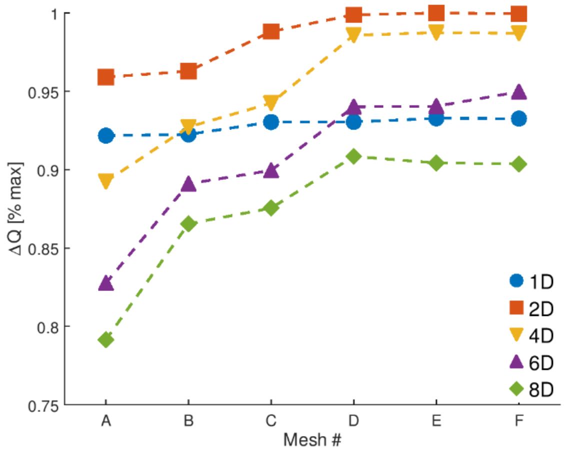

Figure 7. Normalised volumetric flow rate deficit ΔQ in the wake

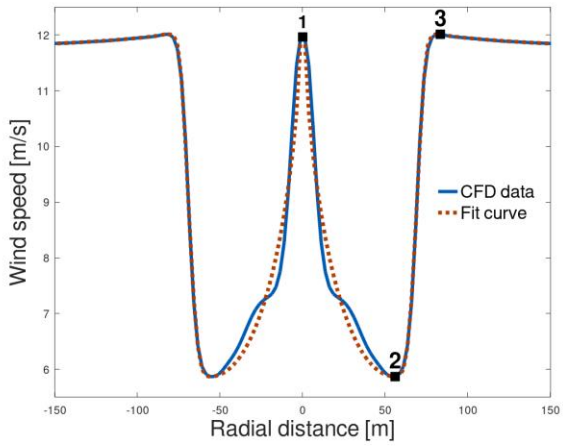

Figure 8. Segmented wake velocity profile with sample fit-curve

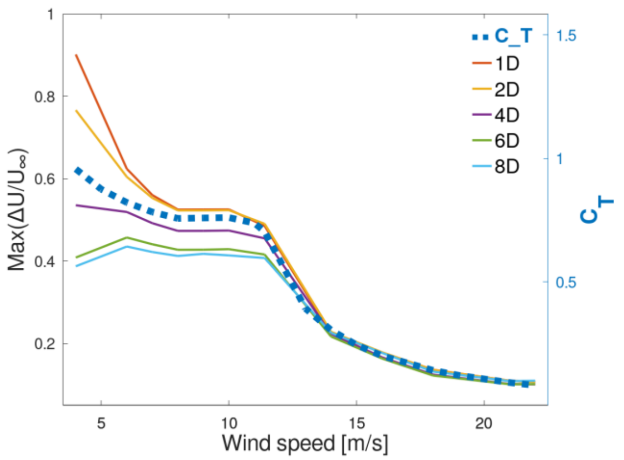

Figure 9. Normalised maximum velocity deficit $\Delta u/U_\infty$ (Node 2) with thrust coefficient C_T overlaid (secondary axis)

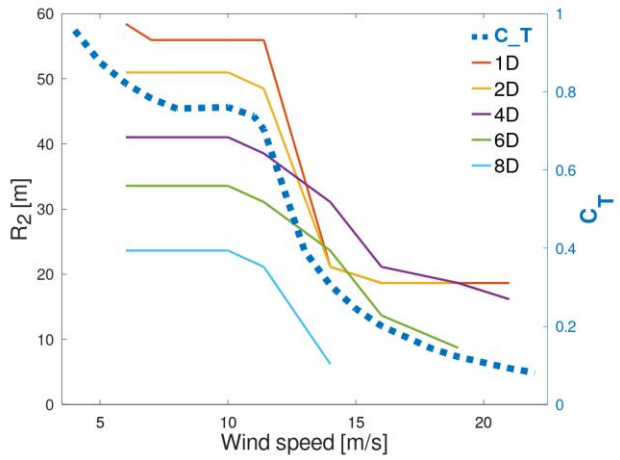

Figure 12. Radial coordinate at $u_{\min}$ (Node 2) with thrust coefficient C_T overlaid (secondary axis)

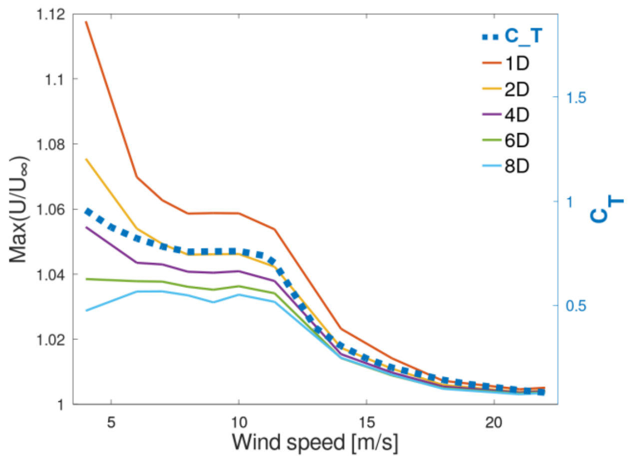

Figure 10. Normalised maximum velocity $u_{\max}/U_\infty$ (Node 3) with thrust coefficient C_T overlaid (secondary axis)

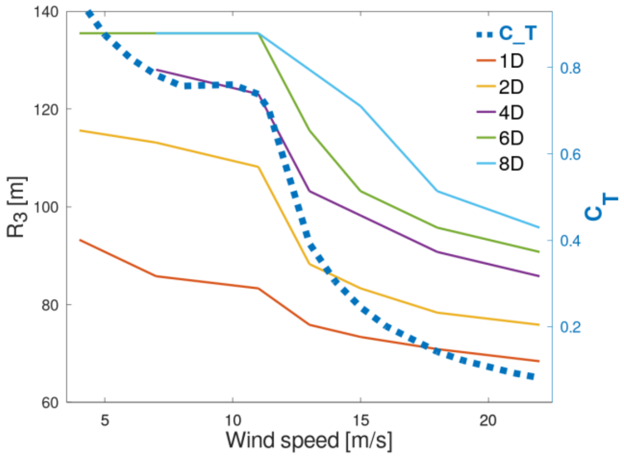

Figure 13. Radial coordinate at $u_{\max}$ (Node 3) with thrust coefficient C_T overlaid (secondary axis)

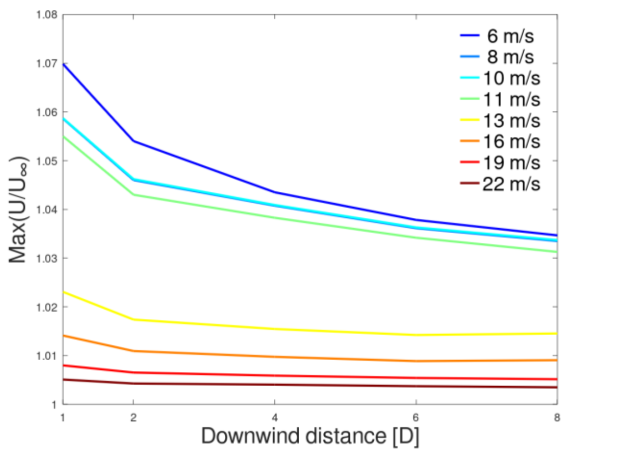

Figure 11. Normalised maximum velocity $u_{\max}/U_\infty$ (Node 3) plotted against downward distance s

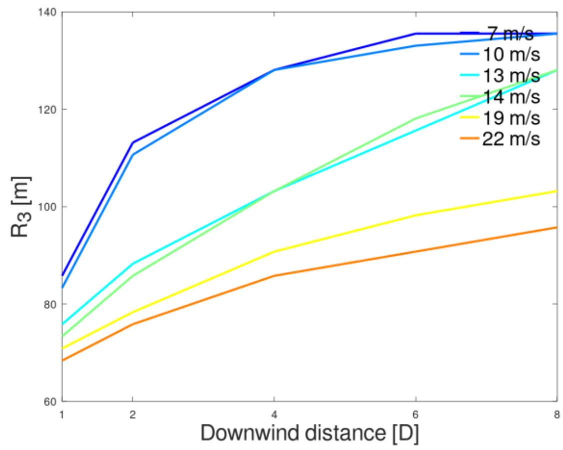

Figure 14. Radial coordinate at $u_{\max}$ (Node 3) plotted against downward distance s

* Please note that the results of our parameterisation study are still pending. The parameterised Node velocity/location results, together with the parameterised regression analysis for exponents a and b in Equation 5, will be presented during the 2020 TwnWEA conference.

III. Case study: Horns Rev I

To investigate the effects of our two tested velocity profiles, we compared the results of a standard Jensen wake model and cosine-distribution Jensen model with operational data recorded by the Supervisory Control and Data Acquisition (SCADA) system of a large-scale wind farm.

The target wind farm for this test was Horns Rev I, located in the North Sea, approximately 14 km off Denmark's west coast. Horns Rev was the world's first large scale offshore wind farm, consisting of 80 Vestas V80-2.0 MW turbines, for a total installed capacity of 160 MW. Construction was completed in 2002, and operational data recorded by the wind farm's SCADA system has since been utilised for several wake model benchmarking studies [14, 15, 16, 17]. The wind farm layout is illustrated in Figure 15.

As discussed in the literature, there is a significant degree of uncertainty in the SCADA data, due to such factors as yaw misalignment of the reference turbine, spatial variability of the wind direction within the wind farm, and wind direction averaging period. It is usually found that this directional uncertainty may be reduced by binning the directional data in sufficiently wide bins [17].

The present study adopted the SCADA data for a westerly wind, i.e. 270° ± 15°. For our test, we took the average of several simulations performed for the same 30° range of "westerly" winds, with 1° steps. The results of this validation test case are shown in Figure 16, which also includes simulated results predicted by Wu et al. [18] using large eddy simulations (LES). The results in Figure 16 are those of the 10 wind turbines in Row D (Figure 15), such that WT #1 is upwind, and does not suffer any wake losses. Accordingly, the energy yields of the nine downwind turbines have been normalised against WT #1. The total output power results for the Horns Rev I Offshore Wind Farm are summarised in Table 3.

Figure 16 shows how the standard Jensen model overestimates the wake losses for the first few downstream turbines, particularly WT #2 to WT #6. For these same few wind turbines, the cosine Jensen model shows excellent agreement with the SCADA site data. However, from WT #7 onwards, both of the Jensen models level off to a constant output, while the site data shows that the output power of the downwind turbines continues to fall. By comparison, the LES data captures the trend fairly well, but is shown to overestimate the output power at all of the downwind turbines.

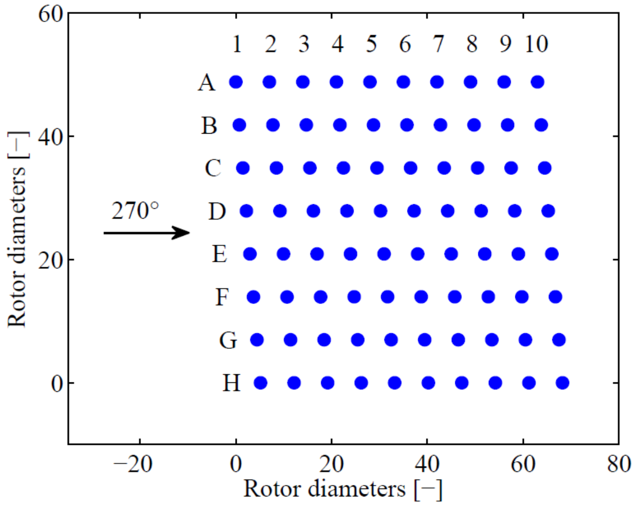

Figure 15. Horns Rev I wind farm layout [14]

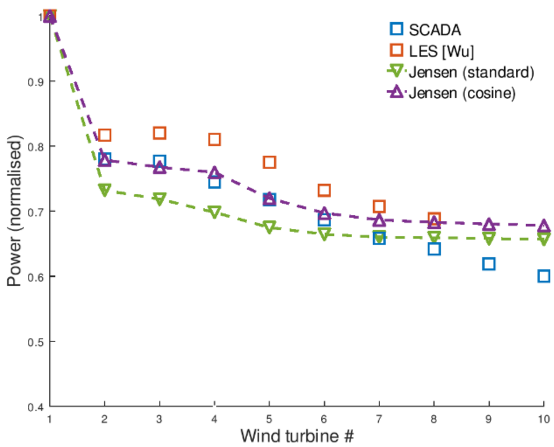

Figure 16. Energy yield results for Horns Rev I OWF (per WT), normalised against WT #1, for wind direction 270° ± 15°

Table 3 Results for Horns Rev I Offshore Wind Farm

Model	Total energy (normalised)	Error [%]
SCADA	0.723	–
LES	0.769	6.5
Jensen (standard)	0.712	1.4
Jensen (cosine)	0.745	3.1

* Please note that the results of our proposed wake model are still pending.

IV. Conclusions

To address the shortcomings of the many analytical wake models which are based on momentum theory, we are currently developing a wake model, derived from unsteady, 3D, full-rotor CFD simulations of the flow field behind a single wind turbine for its full range of operating conditions. This paper describes our CFD model setup, and the parameterisation of our CFD model results, and also describes the two existing wake models against which our analytical model will be compared. In the preliminary stage of this study, we performed several verification tests for the adopted Jensen wake model. The standard Jensen model was shown to correlate extremely well with that employed by the Wind Atlas Analysis and Application Program (WAsP), and comparing two different velocity profiles with SCADA data from a large scale wind farm showed excellent agreement with the SCADA data for the first few downstream turbines, but both wake profiles were shown to underpredict the wake losses in wind turbines farther downstream. Results from our RANS-based parameterised model of the wake profile, which will next be included in our wind farm analysis tool, are to be compared with our Jensen model results.

References

[1] Taiwan Executive Yuan, Four-year Wind Power Promotion Plan,https://english.ey.gov.tw/News3/9E5540D592A5FECD/d603a1bf-9963-4e53-a92b-e6520a3d93ff

[2] The Wake Effect: Impacting turbine siting agreements. North American Clean Energy. http://www.nacleanenergy.com/articles/15348/the-wake-effect-impacting-turbine-siting-agreements

[3] N.O. Jensen, “A note on wind generator interaction”, Roskilde: Risø National Laboratory. Risø-M, No.2411, 1983

[4] B. Nelson, Y. Quéméner, T-Y Lin, “Effects of Wake Meander on Fatigue Lives of Offshore Wind Turbine Jacket Support Structures”, 2018 Taiwan Wind Energy Association Conference, Tainan, Taiwan

[5] van Heemst, J.W., Improving the Jensen and Larsen Wake Deficit Models. Using a Free-Wake Vortex Ring Model to Simulate the Near-Wake. MSc Thesis. TUDelft. 2015

[6] D.J. Renkema, “Validation of wind turbine wake models. Using wind farm data and wind tunnel measurements”, MSc Thesis, TUDelft, Netherlands (2007)

[7] I. Katic, J. Højstrup, N.O. Jensen, “A simple model for cluster efficiency”, European Wind Energy Association Conference and Exhibition, 7-9 October 1986, Rome, Italy, 1986.

[8] F. González-Longatt, P. Wall, V. Terzija. Wake effect in wind farm performance: Steady-state and dynamic behavior. Renew. Energy 39(1), 329–338 (2011).

[9] L-L Tian, W-J Zhu, W-Z Shen, N. Zhao, Z-W Shen, “Development and validation of a new two-dimensional wake model for wind turbine wakes”, Journal of Wind Engineering and Industrial Aerodynamics, 137, 90-99 (2015)

[10] W. Schlez, A. Tindal, D. Quarton, “GH Wind Farmer Validation Report”, Garrad Hassan and Partners Ltd, Bristol, 2003.

[11] H-J Gu, J. Wang, Q. Lin, Q. Gong, “Automatic Contour-Based Road Network Designfor Optimized Wind Farm Micrositing”, IEEE Transactions on Sustainable Energy, Vol. 6, No. 1, 2015

[12] J.Jonkman, S. Butterfield, W. Musial, G. Scott, “Definition of a5-MW Reference Wind Turbine for Offshore System Development”, Technical Report, NREL/TP-500-38060, 2009

[13] WASP User's Manual, https://www.cs.utexas.edu/~ml/wasp/manual.html

[14] K. Hansen, R. Barthelmie, L. Jensen, A. Sommer, “The impact of turbulence intensity and atmospheric stability on power deficits due to wind turbine wakes at Horns Rev wind farm”, Wind Energy, 15:183e96 (2012)

[15] D.R. VanLuvanee, “Investigation of observed and modeled wake effects at Horns Rev using WindPRO”, Master’s thesis, Technical University of Denmark (2006)

[16] R.J. Barthelmie, K. Hansen, S.T. Frandsen, O. Rathmann, J.G. Schepers, W. Schlez, J.A. Phillips, K. Rados, A. Zervos, E.S. Politis, P.K. Chaviaropoulos, “Modelling and measuring flow and wind turbine wakes in large wind farms offshore”, Wind Energy, 12:431e44 (2009)

[17] M. Gaumond, P-E. Réthoré, A. Bechmann, S. Ott, G.C. Larsen, A. Peña, K.S. Hansen, “Benchmarking of wind turbine wake models in large offshore wind farms”, Proceedings of the Science of making torque from wind conference (2012)

[18] Y-T Wu, F. Porté-Agel, “Modeling turbine wakes and power losses within a wind farm using LES: An application to the Horns Rev offshore wind farm”, Renewable Energy, 75, 945-955 (2015).